Equilibrium and Stability of a Circularly Towed Cable Subject to Aerodynamic Drag

J. J. Russell*
United States Air Force Academy, Colorado Springs, Colo.
and
W. J. Anderson†
University of Michigan, Ann Arbor, Mich.

The finite-element method is used to study the equilibrium and stability of an elastic cable whose upper end is towed in a horizontal circular path at a constant angular velocity. Fluid drag is assumed to be composed of tangential and normal components, which are proportional to the tangential and normal velocity components squared, respectively. The problem includes strong geometric nonlinearities and is nonconservative, thereby admitting both static and dynamic instabilities. Equilibrium equations for a cable element including elastogeometric, centripetal, and aerodynamic stiffness matrices are developed in terms of problem parameters and a shape function. All geometric nonlinearities are retained, but small elongations are assumed. The resulting nonlinear algebraic equations are solved using a Newton-Raphson procedure. The stability of an equilibrium position is determined by perturbing the nonlinear equations of motion and calculating the eigenvalues of the resulting linearized dynamic equations. Results indicate multivalued solutions, the number depending on the rotational frequency and tow radius. Both static "jump"-type and dynamic instabilities are found.

Introduction

ALTHOUGH no practical interest has been shown until the last two decades, the equilibrium configuration of a cable towed in a circular path has been of theoretical interest since antiquity. Solutions to the "linearized" eigenvalue problem (zero tow radius) were obtained first by D. Bernoulli (1700-1782) and L. Euler (1707-1783). Work then ceased for two hundred years, until Kolodner's study[1] on the nature of the nonlinear eigenvalue problem. Asymptotic solutions for high rotational frequencies were considered by Wu.[2] Caughey[3] was the first to analyze the nonlinear forced response (nonzero tow radius) and note the similarity of the response to that of a hardening spring-mass system. All authors thus far had considered the towing medium to be a vacuum.

Nate Saint, a missionary working in South America, motivated practical interest in the circularly towed cable idea as a possible aerial delivery system by demonstrating in the early 1950's that a light, fixed-wing aircraft could be used to deliver food and medical supplies to remote villages. He accomplished this by towing a cable with a basket attached to the end from an aircraft orbiting over the delivery point. Surprisingly, the basket hovered almost motionlessly near the ground.

Since then many researchers have studied the problem, introducing new solution techniques and applications. Huang[4] restricted his work to the airborne system but was primarily interested in maximizing the verticality. He was the first to demonstrate the multisolution nature of the problem. Skop and Choo[5] and Crist[6] also considered the equilibrium configuration for the case of aerodynamic drag. Crist[7] studied the effects of crosswind and the transient problems associated with towing the cable into and out of orbit from a rectilinear path. The towing medium was changed from air to water when Choo[8] considered marine applications.

The finite-element method is an extremely powerful approach for problems of this type, since it has the advantages of structural assembly, equivalent nodal load creation, ease of modification, and boundary condition application. The present paper seeks to extend the work of the authors,[9] which employed a linear element to study the circularly towed cable subject to viscous drag, to one subject to aerodynamic drag. Webster[10] since has developed a linear cable element independently, whereas Henghold and Russell[11] have developed a complete family of higher-order cable elements. The equilibrium equations referred to the rotating coordinate system and perturbed equations for small motion about the equilibrium point are developed now for a single element using the principle of virtual work.

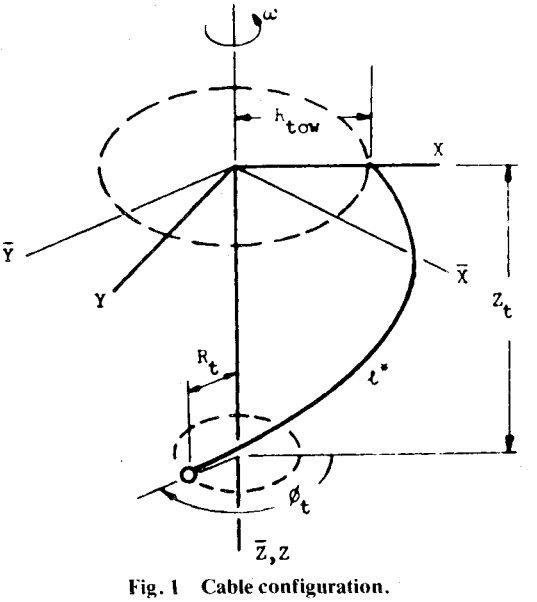

Fig. 1 Cable configuration.

Presented at the AIAA/ASME/SAE 17th Structures, Structural Dynamics, and Materials Conference, King of Prussia, Pa., May 5-7, 1976 (in bound volume of Conference papers, no paper number); submitted May 17, 1976; revision received March 18, 1977.

Index categories: Aeroelasticity and Hydroelasticity; Structural Dynamics; Structural Stability.

*Associate Professor, Department of Civil Engineering, Engineering Mechanics and Materials. Member AIAA.

†Professor of Aerospace Engineering. Member AIAA.

Element Equilibrium

An elastic cable of undeformed length l and mass per unit length m, with its upper end rotated about the Z axis at a constant angular velocity ω, is shown in Fig. 1. The $\bar{X}\bar{Y}\bar{Z}$ system is an inertial reference frame, whereas the XYZ system rotates with the tow point. The final deformed length of the cable is l^*.

The location of any material coordinate in the deformed geometry is

$$\{X^*\} = \{X^*(S)\} \tag{1}$$

where $\{X^*\} = \{X^* Y^* Z^*\}^T$ and S is the undeformed arc length. The velocity $\{v^*\}$ and acceleration $\{a^*\}$ can be written in matrix form as

$$\{v^*\} = [a_I]\{\dot{X}^*\} + \omega[a_G]\{X^*\} \tag{2a}$$

$$\{a^*\} = [a_I]\{\ddot{X}^*\} + 2\omega[a_G]\{\dot{X}^*\} - \omega^2[a_C]\{X^*\} \tag{2b}$$

where $(\dot{})$ indicates differentiation with respect to time, and the following matrices have been defined:

$$[a_I] = \begin{bmatrix} 1\,0\,0 \\ 0\,1\,0 \\ 0\,0\,1 \end{bmatrix} \quad [a_G] = \begin{bmatrix} 0\,1\,0 \\ -1\,0\,0 \\ 0\,0\,0 \end{bmatrix} \quad [a_C] = \begin{bmatrix} 1\,0\,0 \\ 0\,1\,0 \\ 0\,0\,0 \end{bmatrix} \tag{3}$$

Applying the principle of virtual work to a cable element of undeformed arc length L and deformed arc length L^* yields

$$\delta W = \int_0^{L^*} \{\delta X^*\}^T \{f^*\} \mathrm{d}S^* + \{\delta X_N^*\}^T \{r^*\} - \int_0^L A\sigma_s \delta\epsilon_s \mathrm{d}S = 0 \tag{4}$$

where the following terms have been used: ϵ_s, the Lagrangian strain in the deformed axial direction

$$\epsilon_s = \tfrac{1}{2}[(\partial S^*/\partial S)^2 - 1] \tag{5}$$

σ_s, the Kirchoff stress, which is related to ϵ_s through the modulus of elasticity E for a linearly elastic material by

$$\sigma_s = E\epsilon_s \tag{6}$$

A, the undeformed cable cross-sectional area; $\{f^*\}$, the distributed load per unit deformed arc length; $\{X_N^*\}$, the nodal coordinates; and $\{r^*\}$, the corresponding nodal load vector. The shape function $[N]$ relating the coordinates of a generic point to the nodal coordinates then is given by

$$\{X^*\} = [N(S)]\{X_N^*\} \tag{7}$$

where S is measured along the element (see Fig. 2). Using the shape function definition [Eq. (7)], as well as the definitions of ϵ_s [Eq. (5)] and σ_s [Eq. (6)] allows the internal virtual work expression δU to be written in terms of the shape function and nodal coordinates:

$$\delta U = \{\delta X_N^*\}^T \left[\tfrac{1}{2}\int_0^L AE(\{X_N^*\}^T [N']^T [N']\{X_N^*\} - 1) \times [N']^T [N'] \mathrm{d}S\right] \{X_N^*\} \tag{8}$$

The distributed loading $\{f^*\}$ can be decomposed into inertial $\{f_I^*\}$, gravitational $\{f_g^*\}$ and aerodynamic drag $\{f_d^*\}$

$$\{f^*\} = \{f_I^*\} + \{f_g^*\} + \{f_d^*\} \tag{9}$$

where the inertial and gravitational loadings are given by

$$\{f_I^*\} = -m(\partial S/\partial S^*)\{a^*\} \tag{10}$$

$$\{f_g^*\} = mg(\partial S/\partial S^*)\{a_g\} \tag{11}$$

and the column vector $\{a_g\} = \{001\}^T$ for the Z axis aligned with gravity.

The inertial term next is written in terms of the nodal coordinates using Eqs. (2a) and (7). The resulting inertial [Eq. (10)], gravitational [Eq. (11)], and internal virtual work [Eq. (8)] expressions then are substituted into the statement of the principle of virtual work [Eq. (4)] to give

$$[m]\{\ddot{X}_N^*\} + [c_G]\{\dot{X}_N^*\} + [[k_E] - [k_C]]\{X_N^*\} - \{q^*\} = \{g\} + \{r^*\} \tag{12}$$

where the following matrices have been defined:

Consistent mass

$$[m] = \int_0^L m[N]^T [N] \mathrm{d}S \tag{13a}$$

Gyroscopic

$$[c_G] = 2\omega \int_0^L m[N]^T [a_G][N] \mathrm{d}S \tag{13b}$$

Elastogeometric stiffness

$$[k_E] = \tfrac{1}{2}\int_0^L AE(\{X_N^*\}^T [N']^T [N']\{X_N^*\} - 1) \times [N']^T [N'] \mathrm{d}S \tag{13c}$$

Centripetal stiffness

$$[k_C] = \omega^2 \int_0^L m[N]^T [a_C][N] \mathrm{d}S \tag{13d}$$

Gravitational equivalent nodal loads

$$\{g\} = \int_0^L mg[N]^T \{a_g\} \mathrm{d}S \tag{13e}$$

Aerodynamic drag equivalent nodal loads

$$\{q^*\} = \int_0^{L^*} [N]^T \{f_d^*\} \mathrm{d}S^* \tag{13f}$$

The first five of these were evaluated for a linear shape function and are given in an earlier paper by the present authors.[9]

Since the drag force $\{f_d^*\}$ is position- and velocity-dependent, all work with the $\{q^*\}$ vector is motivated so that it is obtained in terms of damping and stiffness-type matrices. The drag force is first decomposed into normal and tangential components.

$$\{f_d^*\} = \{f_t^*\} + \{f_n^*\} \tag{14}$$

where

$$\{f_t^*\} = -\tfrac{1}{2}\rho c_t d^* |v_t^*| \{v_t^*\} \tag{15a}$$

$$\{f_n^*\} = -\tfrac{1}{2}\rho c_n d^* |v_n^*| \{v_n^*\} \tag{15b}$$

The tangential and normal drag coefficients are c_t and c_n, respectively, the deformed cable diameter d^*, the density of air ρ, and the normal and tangential velocity components $\{v_n^*\}$ and $\{v_t^*\}$ are

$$\{v_t^*\} = \left(\{v^*\}^T \left\{\frac{\partial X^*}{\partial S^*}\right\}\right)\left\{\frac{\partial X^*}{\partial S^*}\right\} \tag{16a}$$

or

$$\{v_t^*\} = \left[\left\{\frac{\partial X^*}{\partial S^*}\right\}\left\{\frac{\partial X^*}{\partial S^*}\right\}^T\right]\{v^*\} \tag{16b}$$

and

$$\{v_n^*\} = \{v^*\} - \{v_t^*\} \tag{16c}$$

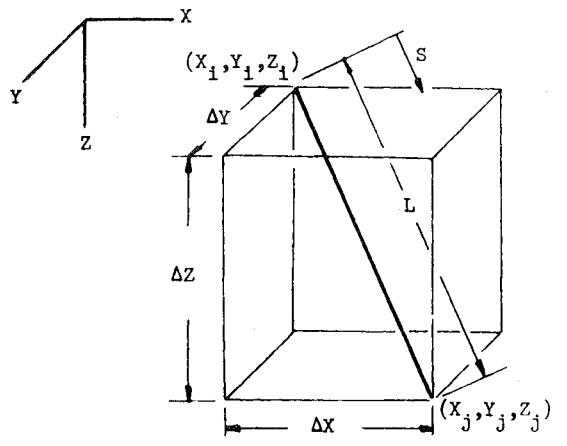

Fig. 2 Linear element.

At this time, only the equilibrium configuration will be considered. Assuming small elemental elongations, S^* can be replaced with S and L^* with L. The equilibrium velocities then can be written in terms of the shape function as

$$\{v\}_0 = \omega[a_G][N]\{X_N\}_0 \tag{17a}$$

$$\{v_t\}_0 = \omega[N']\{X_N\}_0\{X_N\}_0^T[N']^T[a_G][N]\{X_N\}_0 \tag{17b}$$

$$\{v_n\}_0 = \omega([a_G][N] - [N']\{X_N\}_0\{X_N\}_0^T[N']^T[a_G][N])\{X_N\}_0 \tag{17c}$$

where the star superscript has been dropped to indicate the small elongation assumption and the zero subscripts added to denote equilibrium values. Substituting Eq. (17) into the expression for the equivalent nodal loads due to aerodynamic drag yields

$$\{q\}_0 = [k_A]\{X_N\}_0 \tag{18}$$

where the aerodynamic stiffness matrix $[k_A]$ is defined by

$$[k_A] = [k_n^1] + [k_n^2] + [k_t^1] \tag{19}$$

and

$$[k_n^1] = \frac{\omega}{2}\rho c_n d\int_0^L |v_{n_0}|[N]^T[a_G][N]dS \tag{20a}$$

$$[k_n^2] = -\frac{\omega}{2}\rho c_n d\left[\int_0^L |v_{n_0}|[N]^T[N']\{X_n\}_0\{X_N\}_0^T \times [N']^T[a_G][N]dS\right] \tag{20b}$$

$$[k_t^1] = \frac{\omega}{2}\rho c_t d\left[\int_0^L |v_{t_0}|[N]^T[N']\{X_N\}_0 \times \{X_N\}_0^T[N']^T[a_G][N]dS\right] \tag{20c}$$

The values of c_n, c_t, ρ, and d have been assumed to be constant over the element length. The absolute values of the velocity components are calculated from

$$|v_{t_0}| = (\{v_{t_0}\}^T\{v_{t_0}\})^{1/2} \tag{21a}$$

$$|v_{n_0}| = (v_0^2 - (v_{t_0})^2)^{1/2} \tag{21b}$$

These stiffness matrices, which generally are not symmetric, can be evaluated either by using numerical integration or can be integrated analytically if approximate expressions for the velocity magnitudes are employed.

The equilibrium problem then is defined by

$$[k]\{X_N\}_0 = \{g\} + \{r\} \tag{22}$$

where the element stiffness matrix $[k]$ is

$$[k] = [k_E] - [k_C] + [k_A] \tag{23}$$

A discrete approximation to the continuous problem now may be found by assembling cable elements in the standard manner. The resultant stiffness matrix is unsymmetric because of the nonconservative nature of aerodynamic drag. The addition of drogue devices at any node is accomplished easily if drogue lift and drag coefficients are known.

Stability

The stability analysis is based on the infinitesimal motion about a given nonlinear equilibrium position. The presence of nonsymmetric terms in the stiffness matrix requires that a dynamic stability analysis be conducted. A convenient way to obtain the linearized dynamic equations is to perform a variation on the equations of motion for a single element and then assemble the total cable system. From Eq. (12),

$$[m]\{\ddot{\xi}_N\} + [c_G]\{\dot{\xi}_N\} + [[k_E] - [k_C] + [k_L]]\{\xi_N\} - \{\delta q\} = \{0\} \tag{24}$$

where $[k_L]$ is the large deflection stiffness matrix found in Henghold and Russell,[11] and is given by

$$[k_L] = \int_0^L AE[N']^T[N']\{X_N\}_0\{X_N\}_0^T[N']^T[N']dS \tag{25}$$

and the perturbed motion is $\{\xi_N\} = \{\delta X_N\}$.

Evaluating the perturbation of the aerodynamic equivalent nodal loads from Eqs. (13d and 14-16) yields

$$\{\delta q\} = -\tfrac{1}{2}\rho c_n d\int_0^L [N]^T\{v_n\}_0\delta|v_n|dS - \tfrac{1}{2}\rho c_n d\int_0^L |v_{n_0}|[N]^T\{\delta v_n\}dS - \tfrac{1}{2}\rho c_t d\int_0^L [N]^T\{v_t\}_0\delta|v_t|dS - \tfrac{1}{2}\rho c_t d\int_0^L |v_{t_0}|[N]^T\{\delta v_t\}dS \tag{26}$$

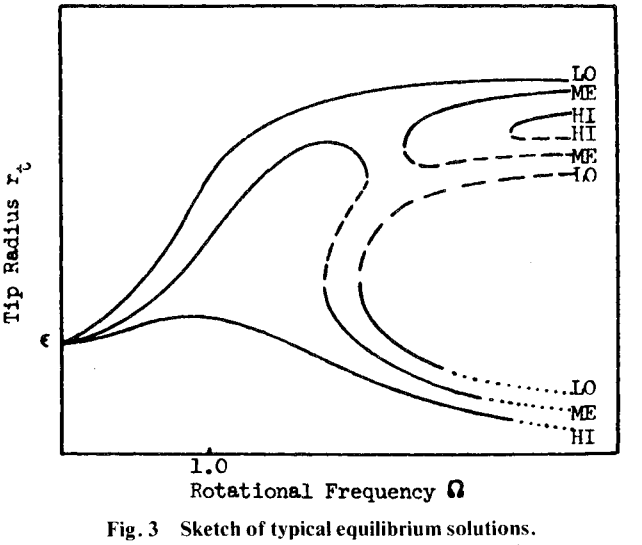

Fig. 3 Sketch of typical equilibrium solutions.

The variations in the absolute velocities are

$$\delta|v_t| = (v_{t_0}/|v_{t_0}|)\delta v_t \tag{27a}$$

$$\delta|v_n| = (v_0/|v_{n_0}|)\delta v + (v_{t_0}/|v_{n_0}|)\delta v_t \tag{27b}$$

Other velocity terms needed to evaluate $\{\delta q\}$ are

$$\{\delta v\} = [a_t][N]\{\dot{\xi}_N\} + \omega[a_G][N]\{\xi_N\} \tag{28a}$$

$$v_0\delta v = \omega\{X_N\}_0^T[N]^T[a_G][N]\{\dot{\xi}_N\} + \omega^2\{X_N\}_0^T[N]^T[a_C][N]\{\xi_N\} \tag{28b}$$

$$\delta v_t = \{X_N\}_0^T[N']^T[N]\{\dot{\xi}_N\} + \omega\{X_N\}_0^T[N']^T[a_G][N]\{\xi_N\} + \omega\{X_N\}_0^T[N]^T[a_G]^T[N']\{\xi_N\} \tag{28c}$$

$$\{\delta v_t\} = \{X_N\}_0^T[N']^T[N']\{X_N\}_0[N]\{\dot{\xi}_N\} + \omega[N'] \times \{X_N\}_0\{X_N\}_0^T[N]^T[a_G]^T[N']\{\xi_N\} + \omega[N']\{X_N\}_0 \times \{X_N\}_0^T[N']^T[a_G][N]\{\xi_N\} + v_{t_0}[N']\{\xi_N\} \tag{28d}$$

Substituting the results of Eqs. (27) and (28) into Eq. (26) yields

$$\{\delta q\} = -[c_A]\{\dot{\xi}_N\} + [k_A - k_{T_A}]\{\xi_N\} \tag{29}$$

where

$$[c_A] = \sum_{i=1}^{6}[c_n^i] + 2[c_t] \tag{30a}$$

$$[k_{T_A}] = \sum_{i=1}^{10}[k_n^i] + 2k_t^1 + 2k_t^2 + k_t^3 \tag{30b}$$

For clarity, the damping matrices and stiffness matrices are listed in the Appendix. Examination of the damping matrices shows that $[c_A]$ is symmetric, as would be expected.

The perturbed equations of motion for an element thus can be written in the form

$$[m]\{\ddot{\xi}_N\} + [c]\{\dot{\xi}_N\} + [k_T]\{\xi_N\} = \{0\} \tag{31}$$

where

$$[c] = [c_G] + [c_A] \tag{32a}$$

$$[k_T] = [k_E] + [k_L] - [k_C] + [k_{T_A}] \tag{32b}$$

Defining $\{\eta_N\}$ as

$$\{\eta_N\} = \begin{Bmatrix} \{\dot{\xi}_N\} \\ \{\xi_N\} \end{Bmatrix} \tag{33}$$

and assuming exponential motion

$$\{\eta_N\} = \{H_N\}e^{\lambda t} \tag{34}$$

leads to the general eigenvalue formulation

$$[A]\{H_N\} = \lambda[B]\{H_N\} \tag{35}$$

where

$$[A] = \begin{bmatrix} [m] & [0] \\ [0] & -[k_T] \end{bmatrix} \quad [B] = \begin{bmatrix} [0] & [m] \\ [m] & [c] \end{bmatrix} \tag{36}$$

Note that the static instability ($\lambda = 0$) is given when the determinant of the tangential stiffness matrix $[k_T]$ is zero.

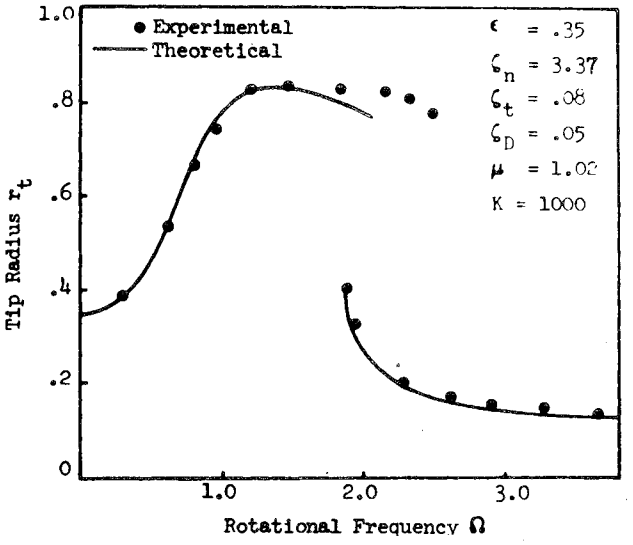

Fig. 4 Frequency response.

Solution Procedure

Since the nonlinearity is primarily of a geometrical nature, a Newton-Raphson procedure is used to solve the equilibrium equation (22). A guess is made to initialize the procedure, and the resulting equilibrium unbalance $[\Psi]$ is calculated from

$$\{\Psi\} = [K]\{X_N\}_0 - \{G\} \tag{37}$$

where $[K]$ and $\{G\}$ are the assembled current stiffness matrix and gravitational equivalent nodal load matrix, respectively. A correction to $\{X_N\}_0$ then is calculated from

$$[K_T]\{dX_N\} = -\{\Psi\} \tag{38}$$

This procedure is repeated until the maximum normalized increment (dX_i/X_i) is smaller than an error index e_c, taken typically to be 0.001. Eigenvalues then are calculated from Eq. (35) using an eigenvalue subroutine based on the *QZ* method to determine the system stability.

After equilibrium and stability calculations have been completed for a given rotational frequency, the value of ω can be incremented by $d\omega$ and a new set of linear equations solved to initialize the iteration procedure at the new frequency. Proceeding in this manner, frequency response curves may be obtained.

Results

The utility of the developed elements now will be demonstrated using the linear element shown in Fig. 2 which has the shape function shown in Eqs. (39). In order to verify these elements,

$$[N] = \begin{bmatrix} 1-S/L & 0 & 0 & S/L & 0 & 0 \\ 0 & 1-S/L & 0 & 0 & S/L & 0 \\ 0 & 0 & 1-S/L & 0 & 0 & S/L \end{bmatrix} \tag{39}$$

theoretical results using approximate expressions for the aerodynamic stiffness, tangential stiffness, and damping matrices are compared to results obtained experimentally. All results are presented in nondimensional form. Spatial coordinates are nondimensionalized with respect to the unstretched cable length, such that the nodal coordinates are given by

$$\{x_N\} = \{X_N/l\} \tag{40}$$

and the tow radius by

$$\epsilon = R_{tow}/l \tag{41}$$

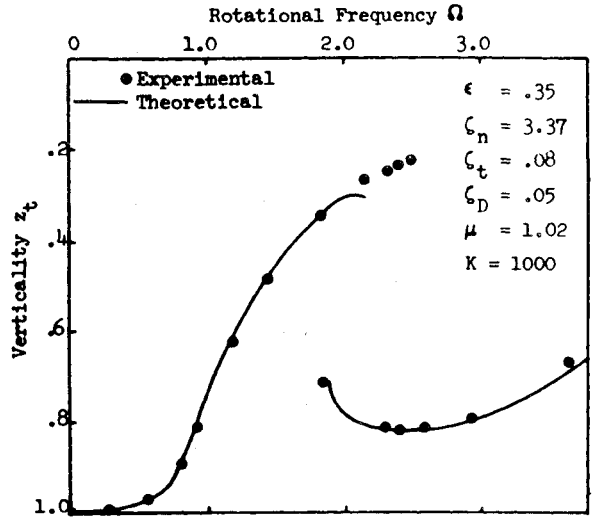

Fig. 5 Verticality.

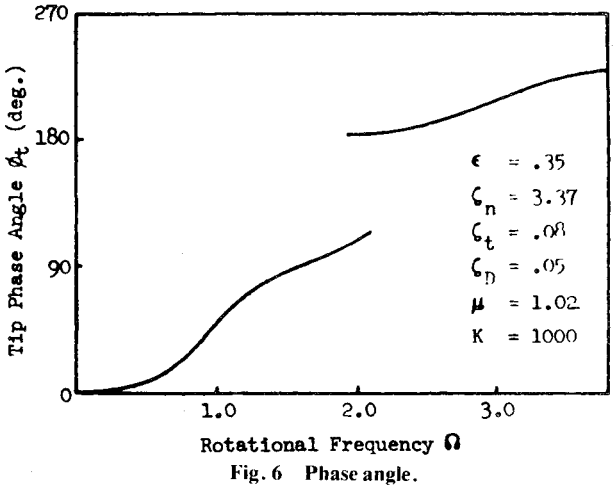

Fig. 6 Phase angle.

Other nondimensionalized variables that are introduced are:

Normal drag coefficient

$$\zeta_n = \tfrac{1}{2}\rho c_n d l/m \tag{42}$$

Tangential drag coefficient

$$\zeta_t = \tfrac{1}{2}\rho c_t d l/m \tag{43}$$

Stiffness to weight ratio

$$K = AE/mgl \tag{44}$$

Rotational frequency

$$\Omega = \omega\sqrt{l/g} \tag{45}$$

The possibility of a spherical drogue at the cable tip has been included. The drogue is characterized by the following two nondimensional parameters:

Drogue drag coefficient

$$\zeta_D = \tfrac{1}{2}\rho c_D A_D/m \tag{46}$$

where c_D is the drogue drag coefficient, considering a drag law in which drag is proportional to the relatively velocity squared. The cross-sectional area of the drogue is A_D.

Drogue to cable mass ratio

$$\mu = M/ml \tag{47}$$

where M is the drogue mass.

Explicit integration of the aerodynamic stiffness, tangential stiffness, and damping matrices is made difficult by the presence of the absolute velocity terms in the integrands. This problem can be overcome either by using numerical integration or by approximating the absolute velocity terms. The second method is used here. The absolute velocities were expanded in a Taylor series in terms of ΔX, ΔY, and ΔZ, where ΔX, ΔY, and ΔZ are just the respective differences in the element end points in each direction. The maximum size of any of these is the element length L. The first two terms were retained in each expansion, these being of order L and L^2 for the aerodynamic stiffness matrices. This expansion is valid for small element elongations and small element size. Lack of space prevents their reproduction in this report. A complete listing appears in Russell.[12]

Equilibrium shapes and their stability are found rather easily and with relatively small computer costs. Overall cable behavior is best described using plots of the three tip parameters: 1) radius r_t, 2) phase angle ϕ_t, and 3) verticality z_t, vs rotational frequency Ω. The tip radius is measured in a horizontal plane from the axis of rotation to the cable tip:

$$r_t = \{[x(1)]^2 + [y(1)]^2\}^{1/2} \tag{48}$$

The phase angle is used to measure the lag of the tip from the tow point and is given by

$$\phi_t = \arctan[y(1)/x(1)] \tag{49}$$

while the verticality is simply the tip value of z

$$z_t = z(1) \tag{50}$$

where all quantities have been defined in nondimensional form. Typical results for three values of drag are sketched in Fig. 3. A hardening spring character is observed with the tow radius ϵ playing the role of the magnitude of the excitation.

For low drag (LO), the system behavior is similar to that of the system without drag. For moderate values of drag (ME), jump phenomena are possible, near the system's first resonant frequency. Also for moderate (ME) and high (HI) values of drag, a detached branch of the equilibrium curve appears in the upper right of the figure. A dynamic stability analysis shows that the dashed portions of the curve are statically unstable, whereas the dotted portions of the curves are dynamically unstable. The qualitative behavior of these solutions and their stability has been confirmed in a related experiment, (Russell[12]).

A typical set of experimental results for a tow radius of 9 in. and cable length of 25.75 in. is used to confirm the theory. The experimental cable model was 0.0185-in.-diam silk thread weighing 4.519×10^{-5} lb/ft. A spherical drogue, with mean diameter of 0.148 in., weighing 9.921×10^{-5} lb, was attached to the cable tip. Since the normal drag coefficient does not vary over a wide range of Reynolds number, c_n was taken as that of a smooth cylinder, $c_n = 1.2$. Even though the tangential drag coefficient does vary with Reynolds number, a constant c_t of 0.01 was used. The drag coefficient for the drogue was taken as that of a sphere, $c_D = 0.47$. Experimental results for tip radius and vertically are shown in Figs. 4 and 5. No experimental phase angle data was obtained.

Theoretical results were obtained using a nine-element cable discretization with the experimental cable parameters. These results are shown in Figs. 4-6. Since no experimental value of K was measured, a value of 1000 was used in the theoretical calculations. Results indicate relative insensitivity to this parameter, except for large tip radii and high rotational frequencies.

Theoretical equilibrium results are, in general, in very good agreement with those obtained experimentally. The only region in which the results disagree is near the jump from large tip radius to small, the theoretical jump occurring

sooner than the actual. Since drag is most important in this region, any differences in theoretical and actual drag coefficients would produce the greatest differences in theoretical and experimental results here. Thus, the discrepancy is explained on the basis of an incorrect estimation of the actual drag.

The stability analysis confirms the zero eigenvalues at the large-to-small and small-to-large radius jumps. The dynamic instability was predicted at $\Omega = 3.08$, although it actually occurred at $\Omega = 3.70$. The discrepancy once more is explained on an incorrect estimation of the drag. Since only the first two eigenvalues were of interest, the nine nodes of the static analysis were condensed to three for the dynamic analysis. No attempt was made to obtain equilibrium solutions in the statically unstable region. Although no upper bound of the unstable region was found for $\Omega < 7.0$ in this case, the bounded behavior has been established for other cases, both experimentally and theoretically.

Conclusions

A finite-element representation of aerodynamic drag acting on a whirling cable has been accomplished. This representation places the position-dependent drag forces in terms of stiffness matrices referred to a rotating reference frame, thus allowing equilibrium solutions to be obtained in the rotating frame. Position-dependent tangential stiffness and damping matrices are used in the perturbed equations of motion. Gravitational, centripetal acceleration, coriolis, and elastic effects also are included in the element. Large cable rotations and position-dependent forces created by the velocity squared drag laws cause the problem to be highly nonlinear.

A computer program has been written for the single whirling cable with a spherical drogue attached to the cable tip. This program has proven to be efficient and capable of coping with multivalued solutions. The Newton-Raphson method is used to find equilibrium positions, and a dynamic perturbation is used to determine the stability of each solution. Modification of the program to solve related problems, such as the whirling cable attached at both ends and the lasso problem, is accomplished easily.

Physical phenomena encountered for the whirling cable include static and dynamic instabilities, jumps from one equilibrium configuration to another, and detached solution branches. The static instabilities and jumps are typical of those observed in damped, hardening, nonlinear, spring-mass systems. The dynamic instability is peculiar to nonconservative systems, whereas the detached branches are rarely seen in the frequency response of mechanical systems. Space has not allowed a study of the effects of the various problem parameters on these phenomena to be included, but a later paper will concentrate on this area.

This paper concentrates on the mathematical development of the aerodynamic portion of a whirling cable element and the solution of a seemingly simple assembly, a single whirling cable. Theoretical results obtained agree with those obtained experimentally. The richness of solutions and associated stability phenomena make it a fascinating study, and impossible to document completely here.

Appendix

The perturbed element aerodynamic damping and stiffness matrices defined in Eq. (30) are given in the following.

Aerodynamic Damping Matrices

$$[c_n^1] = \frac{\omega^2 \rho c_n d}{2}\left[\int_0^L \frac{1}{|v_{n_0}|}[N]^T[a_G][N]\{X_N\}_0 \times \{X_N\}_0^T[N]^T[a_G]^T[N]\mathrm{d}S\right] \quad \text{(A1a)}$$

$$[c_n^2] = \frac{-\omega \rho c_n d}{2}\left[\int_0^L \frac{v_{t_0}}{|v_{n_0}|}[N]^T[a_G][N]\{X_N\}_0 \times \{X_N\}_0^T[N']^T[N]\mathrm{d}S\right] \quad \text{(A1b)}$$

$$[c_n^3] = \frac{\omega \rho c_n d}{2}\left[\int_0^L \frac{v_{t_0}}{|v_{n_0}|}[N]^T[N']\{X_N\}_0 \times \{X_N\}_0^T[N]^T[a_G]^T[N]\mathrm{d}S\right] \quad \text{(A1c)}$$

$$[c_n^4] = \frac{\rho c_n d}{2}\left[\int_0^L \frac{(v_{t_0})^2}{|v_{n_0}|}[N]^T[N']\{X_N\}_0 \times \{X_N\}_0^T[N']^T[N]\mathrm{d}S\right] \quad \text{(A1d)}$$

$$[c_n^5] = \frac{\rho c_n d}{2}\int_0^L |v_{n_0}|[N]^T[N]\mathrm{d}S \quad \text{(A1e)}$$

$$[c_n^6] = \frac{-\rho c_n d}{2}\left[\int_0^L |v_{n_0}|[N]^T[N']\{X_N\}_0 \times \{X_N\}_0^T[N']^T[N]\mathrm{d}S\right] \quad \text{(A1f)}$$

$$[c_t] = \frac{\rho c_t d}{2}\left[\int_0^L |v_{t_0}|[N]^T[N']\{X_N\}_0 \times \{X_N\}_0^T[N']^T[N]\mathrm{d}S\right] \quad \text{(A1g)}$$

Aerodynamic Tangential Stiffness Matrices

$$[k_n^3] = \frac{\omega^3 \rho c_n d}{2}\left[\int_0^L \frac{1}{|v_{n_0}|}[N]^T[a_C][N] \times \{X_N\}_0\{X_N\}_0^T[N]^T[a_C][N]\mathrm{d}S\right] \quad \text{(A2a)}$$

$$[k_n^4] = \frac{-\omega^2 \rho c_n d}{2}\left[\int_0^L \frac{v_{t_0}}{|v_{n_0}|}[N]^T[a_G][N]\{X_N\}_0 \times \{X_N\}_0^T[N]^T[a_G][N']\mathrm{d}S\right] \quad \text{(A2b)}$$

$$[k_n^5] = \frac{-\omega^2 \rho c_n d}{2}\left[\int_0^L \frac{v_{t_0}}{|v_{n_0}|}[N]^T[a_G][N]\{X_N\}_0 \times \{X_N\}_0^T[N']^T[a_G][N]\mathrm{d}S\right] \quad \text{(A2c)}$$

$$[k_n^6] = \frac{-\omega \rho c_n d}{2}\left[\int_0^L v_{t_0}[N]^T[N']\{X_N\}_0 \times \{X_N\}_0^T[N]^T[a_C][N]\mathrm{d}S\right] \quad \text{(A2d)}$$

$$[k_n^7] = \frac{\rho c_n d}{2}\left[\int_0^L (v_{t_0})^2[N]^T[N']\{X_N\}_0 \times \{X_N\}_0^T[N]^T[a_G][N']\mathrm{d}S\right] \quad \text{(A2e)}$$

$$[k_n^8] = \frac{\rho c_n d}{2}\left[\int_0^L (v_{t_0})^2[N]^T[N']\{X_N\}_0 \times \{X_N\}_0^T[N'][a_G][N]\mathrm{d}S\right] \quad \text{(A2f)}$$

$$[k_n^9] = \frac{-\omega\rho c_n d}{2}\left[\int_0^L |v_{n_0}|[N]^T[N']\{X_N\}_0 \times \{X_N\}_0^T[N]^T[a_G]^T[N']\mathrm{d}S\right] \quad \text{(A2g)}$$

$$[k_n^{10}] = \frac{\rho c_n d}{2}\int_0^L v_{t_0}|v_{n_0}|[N]^T[N']\mathrm{d}S \quad \text{(A2h)}$$

$$[k_t^2] = \frac{\rho c_t d}{2}\left[\int_0^L |V_{t_0}|[N]^T[N']\{X_N\}_0 \times \{X_N\}_0^T[N]^T[a_G][N']\mathrm{d}S\right] \quad \text{(A2i)}$$

$$[k_t^3] = \frac{\rho c_t d}{2}\int_0^L (v_{t_0})^2[N]^T[N']\mathrm{d}S \quad \text{(A2j)}$$

References

[1] Kolodner, I. I., "Heavy Rotating String – A Nonlinear Eigenvalue Problem," *Communications on Pure and Applied Mathematics*, Vol. VIII, 1955, pp. 334-338.

[2] Wu, C. H., "Whirling of a String at Large Angular Speeds – A Nonlinear Eigenvalue Problem with Moving Boundary Layers," *SIAM Journal of Applied Mathematics*, Vol. 22, No. 1, Jan. 1972, pp. 1-13.

[3] Caughey, T. K., "Whirling of a Heavy Chain," *Proceedings of the Third U.S. National Congress of Applied Mechanics*, 1958, pp. 61-108.

[4] Huang, J., "Mathematical Model for Long Cable Towed by Orbiting Aircraft," U.S. Naval Air Development Center Rept. NADC-AM-6849, June. 1969.

[5] Skop, R. A. and Choo, Y., "The Configuration of a Cable Towed in a Circular Path," *Journal of Aircraft*, Vol. 8, Nov. 1971, pp. 856-862.

[6] Crist, S. A., "Analysis of the Motion of a Long Wire Towed from an Orbiting Aircraft," *The Shock and Vibration Bulletin*, Bull. 41, Dec. 1970, pp. 61-73.

[7] Crist, S. A., "Steady State Shape of Orbiting Trailing Wire System," United States Air Force Academy Research Rept. 72-8, Oct. 1972.

[8] Choo, Y. and Casarella, M. J., "Configuration of a Towline Attached to a Vehicle Moving in a Circular Path," *Journal of Hydronautics*, Vol. 6, Jan. 1972, pp. 51-57.

[9] Russell, J. J. and Anderson, W. J., "Whirling Cable Subjected to Viscous Drag," *Proceedings of the 1974 International Conference on Finite Element Methods in Engineering*, The University of New South Wales, pp. 661-676.

[10] Webster, R. L., "Structural Response of Arbitrary Underwater Cable Systems," *Ocean Engineering Mechanics*, OED-Vol. 1, American Society of Mechanical Engineers, New York, 1975, pp. 43-59.

[11] Henghold, W. M. and Russell, J. J., "Equilibrium and Natural Frequencies of Cable Structures (A Nonlinear Finite Element Approach)," *Proceedings of the Second National Symposium on Computerized Structural Analysis and Design*, March 1976.

[12] Russell, J. J., "Equilibrium and Stability of a Whirling Cable," Ph.D. Dissertation, The University of Michigan, 1974 (University Microfilms).